

Origin of the maximal critical temperature disparities in one - layer cuprate superconductors.

Baruch Rosenstein¹ and B. Ya. Shapiro²

¹*Electrophysics Department, National Yang Ming Chiao Tung University, Hsinchu 30050, Taiwan, R. O. C**

²*Physics Department, Bar-Ilan University, 52900 Ramat-Gan, Israel[†]*

Recently a phonon exchange d - wave pairing mechanism in cuprates was proposed. The phonons are the lateral apical oxygen atoms vibrations. They generate the attractive pairing potential peaked at Γ point of the Brillouin zone, $V(k) \propto \exp[-2kd_a]$, where d_a is distance from the CuO planes. The model explains a rather paradoxical well known negative correlation of the optimal doping critical temperature T_c^{\max} with d_a and increase of T_c^{\max} with pressure. However the large disparities in T_c^{\max} , especially in one - layer cuprate superconductors, from 39K for $La_{2-x}Sr_xCuO_4$, to 95K for $HgBa_2CuO_{4+\delta}$, cannot be attributed by differences in d_a . Other important material parameters include the hopping amplitudes t, t' and the on site Coulomb repulsion U . It is shown (within weak coupling).that T_c^{\max} is highest for materials close to the topological (Lifshitz) transition from an open to a close Fermi surface. The transition occurs for $t' = -0.19t$ and rather small values of effective value of $U = 2t$ at optimal doping. Analytic expressions for T_c^{\max} are derived both near criticality and away from it.

PACS numbers: PACS: 74.20.Rp, 74.72.-h, 74.25.Dw

I. INTRODUCTION

The physical cause of high temperature superconductivity in cuprates is still under intensive debate despite enormous body of experimental facts and numerous theoretical proposals. It is generally accepted that the normal state including the Mott anti - ferromagnetic (AF) insulator at low doping, the pseudogap and strange metal phases at intermediate dopings are due to strong on site electron repulsion U in the CuO_2 planes. Since the pairing is d-wave, it was conjectured that an in - plane mechanism like the AF spin fluctuations play a major role. One of the obvious questions one asks about the pairing mechanism in cuprates¹ is why structurally identical members of the cuprate family like the one - layered $La_{2-x}Sr_xCuO_4$ ("La") and $HgBa_2CuO_{4+\delta}$ ("Hg") have so different maximal critical temperatures (39K and 95K respectively). A purely CuO mechanism when applied to whole family of cuprates raises several questions. Moreover it is believed now that La has *larger* U than Hg, so that a weaker coupled system develops much larger pairing than an "iconic" strongly coupled system La.

Recent first principle calculations provide increasingly accurate estimates of U that should be used in Hubbard - like modeling on the "mesoscopic" scale. Limiting ourselves to simplest one - layer cuprates, one estimates² $U = 6.5t$ for lower T_c parent compounds La_2CuO_4 and $Bi_2Sr_2CuO_6$, while the highest T_c^{\max} compounds, Hg and $Tl_2Ba_2CuO_6$ have smaller on site Coulomb repulsion $U = 4.5t$, see Table 1. The nearest neighbors hopping is roughly the same ($t = 450 - 470meV$) for all the materials. Other recent calculations³ give slightly larger values of U , but ratios of U for various materials are the same. The critical temperature is maximal at the universal hole doping, $p_{opt} \simeq 0.16$, for the four compounds. In the framework of "unconventional" pairing mechanism (as the spin fluctuations within the CuO layer) the disparity in critical temperature is counter - intuitive: stronger correlations should lead to larger T_c^{\max} at least in the intermediate coupling (namely $U < W$, where the bandwidth is $W \simeq 5 - 8t$). At very large U the dependence of T_c^{\max} is not clear. Other presumably important characteristics of these materials in addition to t and U are the apical distance and the next to nearest hopping amplitudes determining the dispersion relation.

The structure of the compounds is quite similar. The lattice spacing is almost the same, $a = 3.8 - 3.9A$, while the two apical oxygen atoms are above and below the Cu atoms. These distances are $d_a = 2.4A$ for the low T_c materials (La, Bi) and $d_a = 2.8A$ for higher T_c (Hg,Tl), see Table 1. Correlation of T_c^{\max} with apical distance d_a (despite the small differences between materials) and the next to nearest neighbor hopping, t' , was noticed early on in numerous cuprate families⁴. On the basis of ARPES measurement it was noted¹, that near the optimal doping the Fermi surfaces have different topology: the diamond shape ("closed") for La and Bi, while it is hyperbolically ("open") for Hg and Tl, see Fig.1. This fact was first to blame for a factor 2.5 disparity in critical temperature. To quote¹: "Since the size of the superconducting gap is largest in the antinodal region, differences in the band dispersion at the antinode may play a significant role in the pairing and therefore affect the maximum transition temperature". This is also qualitatively in accord with values of t' estimated⁴, $|t'|/t = 0.17$ in La and 0.33 in Hg since at certain value of t'/t there is a topological (Lifshitz) transition from an open to close Fermi surface, see Fig.1, where the FS for $p_{opt} = 0.16$ is given for five values of t' . It is not clear how close the two materials are to the topological transition point (center panel in Fig.1), but apparently La,Bi are far from it (on the left), while Tl,Hg are much closer (the right) to the transition.

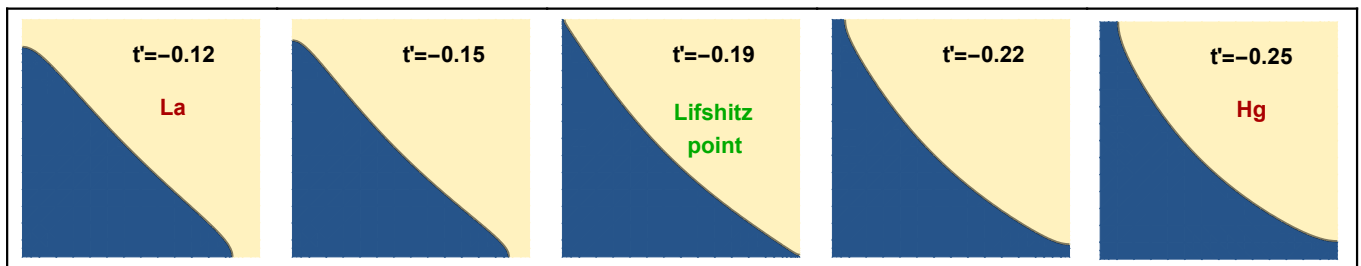


FIG. 1. Fermi surface (in the first quarter of the BZ) of the tight binding binding model at fixed doping (here the universal optimal doping $p=0.16$). Topological transition occurs on the central frame. FL is closed around the Γ point on the left, while open (equivalently centered at the M point) on the right.

An idea that the peak in T_c appears on the topological transition line is not unique to the high T_c cuprates. For example it was predicted⁵ that when a Weyl semimetal undergoes a Lifshitz transition from the type I (closed FS, elliptic) to the type II (open FS, hyperbolic) such a peak (the s-wave) should appear. It was observed in $HfTe_5$ by applying pressure⁶. The main reason is clearly the spectral weight enhancement at points at which the pairing occurs. Returning to cuprates, one notices that at the open - close transition FS passes the van Hove point $\mathbf{X} = (\pi, 0)$ of the BZ, see central frame in Fig.1, The van Hove singularity in cuprates was observed experimentally⁷. Theoretically the van Hove singularity's effect on the s - wave superconductivity was studied⁸ (in some cases in relation to cuprates⁹), but the result was that the enhancement was found to be negligible.

The question of the superconductivity dependence on the dispersion relation (like tuning t' to the van Hove singularity) within the spin fluctuation pairing theory typically based on the Hubbard model was not addressed for a number of reasons. First it has not been convincingly established that the model has the d - wave ground state around p_{opt} . The weak coupling, $U < 4t$, just leads to an exponentially small d - wave instability¹⁰, while recently it was demonstrated that at strong coupling, $U > 5t$, competing correlated states take over¹¹). Second, the strongly coupled theory requires application of very complicated methods¹² that makes a delicate fine tuning of the band parameters nearly impossible.

Recently a phonon exchange d - wave pairing mechanism in cuprates was proposed¹³. It was argued that the only phonon modes capable of generating the d -wave pairing in the CuO plane are the lateral apical oxygen atoms vibrations. Better studied the in - plane breathing and buckling oxygen vibrations¹⁴ and the apical oxygen c - direction modes¹⁵ are not able to generate a significant d-wave T_c . The apical lateral oxygen vibrations in ionic environment generate¹³ an attractive pairing in - plane potential, $V(k) \propto \exp[-2kd_a]$. This phonon exchange model will be referred to as ALLP. The d_a dependence explains a well known correlation of the optimal doping critical temperature T_c^{max} with pressure, but, as mentioned above is impossible to explain the large disparities in T_c^{max} .

The model at intermediate U describes well¹³ various normal properties in the doping range not too close to the Mott insulator. In an underdoped cuprate (with locally anti - ferromagnetic pseudogap) FS have four Fermi pockets, while the transition to the overdoped samples occurs via the Lifshitz point (optimal doping, *different* from the open - close FS Lifshitz transition discussed above) where the pockets coalesce into a single Fermi surface. Importantly the phonon generated T_c is maximal at the optimal doping, where the pseudogap disappears. In the overdoped strange metal linear in temperature resistivity was obtained¹⁶.

In the present paper we apply the ALLP of the d - wave superconductivity at optimal doping in the case when the system is near the open-close FS topological transition. The main feature in this case is that of the Fermi surface approaches the van Hove singularity point \mathbf{X} . In particular it paradoxically results in the largest T_c^{max} for materials with lowest U . The paper is organized as follows. In Section II a model of the lateral optical phonons in ionic crystal and an effective $t - t'$ model of the correlated electron gas is presented. This 50mev phonon mode and its coupling including the matrix elements are described sufficiently well by the Born - Meyer approximation that has been applied to cuprates¹⁷. In Section III symmetrized Hartree - Fock approximation¹⁸ (valid for intermediate strength U) is used to investigate the Fermi surface topology change. We concentrate on the optimal doping and consider the topological close to open Fermi surface transition. In Section IV we develop a BCS - like d - wave theory of superconductivity in the framework of dynamic approach. The effect of the van Hove singularity is taken into account approximately. Section V contains results for different one - layer cuprates obtained directly from numerical solution of Gorkov equations. In the last Section results are summarized and discussed.

II. THE MODEL

Our model consists of the 2DEG interacting with phonons of a polar insulator:

$$H = H_e + H_{ph} + H_{e-ph}. \quad (1)$$

We start with the phonon term. The electron part is the Hubbard model, while the coupling between the electronic and vibrational degrees of freedom, H_{e-ph} , is subject of the last Subsection.

A. The apical oxygen lateral vibrations contribution to the effective electron - electron interaction

Although the prevailing hypothesis is that superconductivity in cuprate is "unconventional", namely not to be phonon - mediated, the phonon based mechanism has always been a natural option to explain extraordinary superconductivity in cuprates. The crystal has very rich spectrum of phonon modes. However very few have a strong coupling to 2DEG and even fewer can generate lateral (in plane) forces causing pairing. As mentioned in Introduction,

TABLE I. Material parameters of one layer cuprates.

| material | $La_{2-x}Sr_xCuO_4$ | $Bi_2Sr_2CuO_{6+\delta}$ | $HgBa_2CuO_{4+\delta}$ | $Tl_2Ba_2CuO_{6+\delta}$ |
|----------------|---------------------|--------------------------|------------------------|--------------------------|
| T_c^{opt} | 39 | 35 | 95 | 95 |
| U_{parent}/t | 6.5 | 4.06 | 3.93 | 3.82 |
| U_{opt}/t | 2.6 | 2.7 | 1.9 | 1.9 |
| t'/t | -0.13 | -0.12 | -0.19 | -0.20 |
| d_a [Å] | 2.4 | 2.45 | 2.79 | 2.7 |

the most studied phonon "glue" mode has been the oxygen vibrations within the CuO plane¹⁴. It was argued¹⁹ (in the context of high T_c 1UC $FeSe$ on perovskite substrates where this was observed experimentally²⁰) that lateral vibrations of the oxygen atoms in the adjacent ionic perovskite layer can couple strongly to 2DEG residing in the CuO plane.

The structure of the La_2CuO_4 and $HgBa_2CuO_6$ unit cell below the conducting layer is schematically depicted in Fig. 2. Besides the single CuO_2 (Cu is drawn in Fig.2 as a brown sphere, O - small orange spheres).layer only two insulating oxide layers are assumed to be relevant. The closest layer at distance d_a , see Table I, consists of heavy Ba atoms (cyan rings) and light "apical" oxygen (small red circle). The next layer is LaO/HgO , (Hg - violet, O - small dark red circles). Qualitatively one of the reasons is that the LaO/BaO layer, see Fig. 2, constitutes a strongly coupled ionic insulator. Unlike the metallic layer where screening is strong, in an ionic layer screening is practically absent and a simple microscopic theory of phonons and their coupling exists²¹. Although phonons in cuprates were extensively studied within the first principle approach including the oxygen vibration mode the matrix elements are rarely discussed, so that the simple approach is appropriate¹⁷. It was repeatedly noticed²² that vibrations in c directions contribute little to the in - plane pairing.

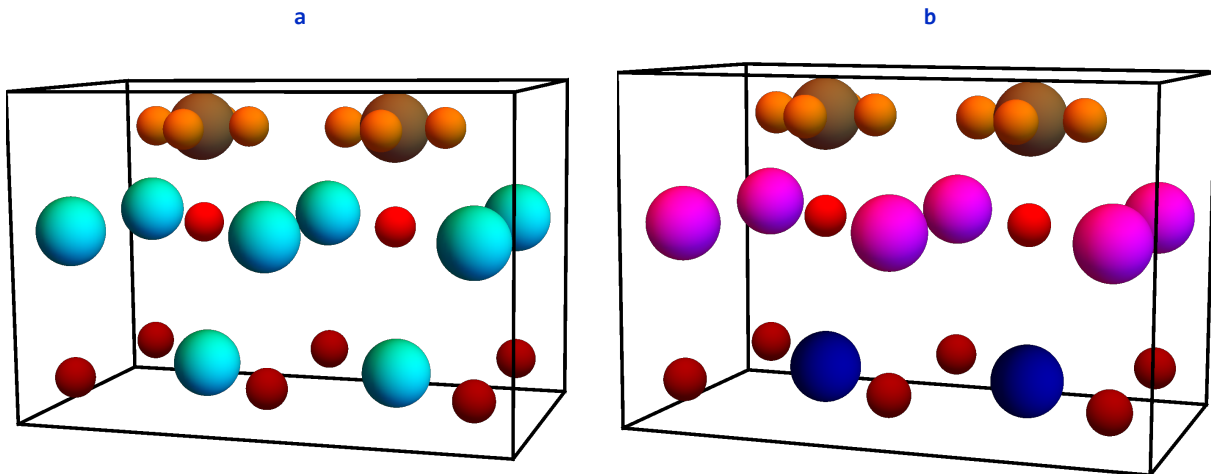


FIG. 2. The profile 3D view of three layers comprising relevant part of the one unit cell :of La_2CuO_4 and $HgBa_2CuO_6$. The top is the CuO_2 (Cu - brown sphere, O - orange), ALLP are located inthe insulating LaO/BaO (La -cyan Ba - magenta violet) O (dark red). The third layer: LaO/HgO , (Hg - violet, O - red). Sizes of atoms are inversely proportional to the values of the Born - Mayer inter - atomic potential parameter parameter b

Phonons in ionic crystals are described sufficiently well by the Born - Meyer potential due to electron's shells repulsion²¹ and electrostatic interaction of ionic charge,

$$V(r) = \sqrt{A_1 A_2} \exp \left[-\frac{1}{2} (b^1 + b^2) r \right] + Z_1 Z_2 \frac{e^2}{r}, \quad (2)$$

with standard values of coefficients A and b for all the atoms. The ionic charges Z are estimated from the DFT calculated Milliken charges²³ or determined phenomenologically. In the LaO/BaO layer the charges are constrained

by neutrality. Since oxygen is much lighter than La/Ba , the heavy atoms' vibrations are negligible. Obviously that way we lose the acoustic branch, however it is known that the acoustic phonons contribute little to the pairing²². Atoms in neighboring layers can also be treated as static. Moreover one can neglect more distant layers. Even the influence of the yet lower layers (below the last layer shown in Fig. 2) is insignificant due to the distance. Consequently the dominant lateral displacements, $u_{\mathbf{m}}^{\alpha}$, $\alpha = x, y$, are of the oxygen atoms directly beneath the Cu sites at $\mathbf{r}_{\mathbf{m}} = a(m_1, m_2)$.

The dynamic matrix $D_{\mathbf{q}}^{\alpha\beta}$ is calculated by expansion of the energy to second order in oxygen displacement (details in Appendix A in ref.¹³), so that the phonon Hamiltonian in harmonic approximation is:

$$H_{ph} = \frac{1}{2} \sum_{\mathbf{q}} \left\{ M \frac{du_{-\mathbf{q}}^{\alpha}}{dt} \frac{du_{\mathbf{q}}^{\alpha}}{dt} + u_{-\mathbf{q}}^{\alpha} D_{\mathbf{q}}^{\alpha\beta} u_{\mathbf{q}}^{\beta} \right\}. \quad (3)$$

Here M is the oxygen mass. Summations over repeated components indices is implied. Now we turn to derivation of the phonon spectrum. Two eigenvalues, the transversal optical (TO) and the longitudinal optical (LO) modes are given in obtained. One observes that there are longitudinal modes are in the range $\Omega_{\mathbf{q}} \sim 45 - 511 meV$ and $25 - 32 meV$ respectively. The energy of LO modes is larger than that of the corresponding TO, although the sum $\Omega_{\mathbf{q}}^{LO} + \Omega_{\mathbf{q}}^{TO}$ is nearly dispersionless. At Γ the splitting is small, while due to the long range Coulomb interaction there is hardening of LO and softening of TO at the BZ edges. The dispersion of the high frequency modes is small, while for the lower frequency mode it is more pronounced.

B. The $t - t'$ Hubbard model of the 2DEG in CuO layers.

The electron gas is described by an effective single band $t - t'$ model. Hamiltonian in momentum space is:

$$H_e = \sum_{\mathbf{k}} c_{\mathbf{k}}^{\sigma\dagger} (\epsilon_{\mathbf{k}} - \mu) c_{\mathbf{k}}^{\sigma} + U \sum_{\mathbf{i}} n_{\mathbf{i}}^{\uparrow} n_{\mathbf{i}}^{\downarrow}, \quad (4)$$

Here $c_{\mathbf{k}}^{\sigma\dagger}$ is the electron creation operator with spin projection $\sigma = \uparrow, \downarrow$. Only nearest and next to nearest neighbors hopping terms are included:

$$\epsilon_{\mathbf{k}} = -2t (\cos[ak_x] + \cos[ak_y]) - 4t' \cos[ak_x] \cos[ak_y]. \quad (5)$$

The dispersion relation thus is simplified with respect to a "realistic" one in which more distant hops are included. The on site repulsion is described by the on site Hubbard repulsion term with $n_{\mathbf{i}}^{\sigma} = c_{\mathbf{i}}^{\sigma\dagger} c_{\mathbf{i}}^{\sigma}$ being the spin σ occupation on the site $\{i_x, i_y\}$ and μ is the chemical potential. Due to the repulsion, even the model without phonons is nontrivial and will be treated approximately in the next Section. Now we turn to the electron - phonon coupling.

C. Electron - phonon coupling

The lateral apical oxygen phonon's interaction with the 2DEG on the adjacent CuO layer d_a above the LaO/BaO plane is determined by the electric potential created the charged apical oxygen vibration mode $\mathbf{u}_{\mathbf{m}}$ at arbitrary point \mathbf{r} is:

$$\Phi(\mathbf{r}) = \sum_{\mathbf{m}} \frac{Ze}{\sqrt{(\mathbf{r} - \mathbf{r}_{\mathbf{m}} - \mathbf{u}_{\mathbf{m}})^2 + d_a^2}}, \quad (6)$$

The apical oxygen charge was taken as $Z = 1.3$. The electron-phonon interaction (EPI) Hamiltonian that accounts for the hole charge distribution in the CuO plane is derived in Appendix A of ref.¹³. The result in momentum space has a density - displacement form

$$H_{eph} = Ze^2 \sum_{\mathbf{q}} n_{-\mathbf{q}} g_{\mathbf{q}}^{\alpha} u_{\mathbf{q}}^{A\alpha}, \quad (7)$$

with EPI matrix element,

$$\mathbf{g}_{\mathbf{q}} = 2\pi\hat{\mathbf{q}} e^{-|q|d_a}. \quad (8)$$

Here $|\mathbf{q}|^2 \equiv 4 (\sin^2 [q_x/2] + \sin^2 [q_y/2])$. It is well known that only longitudinal phonons contribute to the effective electron - electron interaction, as is clear from the scalar product form of the Eq.(7). The precision of the last equality is 2%, see figure 9,10 in Appendix A of ref.¹³.

To conclude Eqs.(4,3,7) define our microscopic model. Now we turn to description of the normal state

III. TUNING TO THE OPEN - CLOSE FERMI SURFACE TRANSITION

A. Mean field description of the Hubbard model at intermediate coupling

The normal state of cuprates exhibits a host of phenomena including pseudogap in underdoped regime resulting in fracture of the Fermi surface. In the intermediate to weak coupling range, $U/t = 1 - 2.5$, one can use a much simpler approximation scheme: the Hartree - Fock approximation with its extension including the RPA type coupling U renormalization^{13,24} and symmetrized HF¹⁸. It provides a good agreement with the more sophisticated methods. The coupling U that enters the Hubbard description generally depends on doping. It is largest for the parent material (Mott insulator in all holed doped cuprates). The first principle values were given in Introduction. However in the present paper we focus on the optimal doping $p_{opt} = 0.16$ for which the value \bar{U} is significantly reduced. In some first principle calculations doping is simulated by periodic substitution. For example the band structure of the $p = 0.25$ La was simulated recently²⁵. As discussed above host of normal and superconducting properties in overdoped, optimal and slightly underdoped materials can be described in the intermediate coupling regime.

Generally the HF approximation takes into account the ground state reconstruction due to the electron - hole pairs generated by the Coulomb repulsion. In translation invariant case it results in renormalization of the chemical potential

$$\mu_r = \mu - Un/2. \quad (9)$$

Within the HF approximation the density at temperature T at optimal (and above) doping is related to the dispersion relation and chemical potential μ by

$$n = \frac{2}{(2\pi)^2} \int_{BZ} \frac{1}{1 + \exp [(\epsilon_{\mathbf{k}} - \mu_r)/T]}. \quad (10)$$

From now on we chose units in which $a = t = \hbar = 1$.

Let us find the value of parameters at which the renormalized FS "reaches" the van Hove singularity point $\mathbf{X} = (\pi, 0)$, $\epsilon_{\mathbf{X}} - \mu_r = 0$. As can be seen from Fig.3c and Fig.1, precisely at this value the electronic system undergoes a Lifshitz transition from closed FS (like in La) to an open one (like in Hg). For our dispersion relation, Eq.(5), this becomes

$$\mu_r = \epsilon_{\mathbf{X}} = 4t'. \quad (11)$$

At this point Eq.(10) depends on t' only:

$$n = \frac{2}{(2\pi)^2} \int_{BZ} \frac{1}{1 + \exp [(\epsilon_{\mathbf{k}} - \epsilon_{\mathbf{X}})/T]}. \quad (12)$$

The doping $p = 1 - n$ is given for $T = 0.02 t$ in Fig.3. It is almost independent of temperature for $T < 0.1 t \approx 500K$ for $t = 450 meV$ and allows a linear fit, $p = 0.84 t'/t$. In particular for the optimal doping $p = 0.16$ one should have $t' = -0.19 t$. If the Tl and Hg cuprates are very close to the transition due their high T_c^{max} , they should have this value of the next to nearest neighbor hopping.

The assumption that the doping is optimal means that it obeys an additional equation for the AF-paramagnet criticality (assuming the second order transition), see ref.¹³. This determines U as the following integral over the magnetic BZ:

$$U^{-1} = \frac{1}{4(2\pi)^2} \int_{k_1=0}^{\pi} \int_{k_y=-\pi}^{\pi} \frac{1}{|h_{\mathbf{k}}|} \left(\tanh \left[\frac{\epsilon'_{\mathbf{k}} - \mu_r + |h_{\mathbf{k}}|}{2T} \right] - \tanh \left[\frac{\epsilon'_{\mathbf{k}} - \mu_r - |h_{\mathbf{k}}|}{2T} \right] \right) \quad (13)$$

Here $k_1 = k_x - k_y$ and,

$$\begin{aligned} h_{\mathbf{k}} &= 1 + e^{i(2k_1)} + e^{ik_y} + e^{i(2k_1 - k_y)}; \\ \epsilon'_{\mathbf{k}} &= -4t' \cos [k_1] \cos [k_1 - k_y]. \end{aligned} \quad (14)$$

At van Hove chemical potential it takes a form:

$$U^{-1} = \frac{1}{4(2\pi)^2} \int_{k_1=0}^{\pi} \int_{k_y=-\pi}^{\pi} \frac{1}{|h_{\mathbf{k}}|} \left(\tanh \left[\frac{\varepsilon'_{\mathbf{k}} - 4t' + |h_{\mathbf{k}}|}{2T} \right] - \tanh \left[\frac{\varepsilon'_{\mathbf{k}} - 4t' - |h_{\mathbf{k}}|}{2T} \right] \right) \quad (15)$$

This gives the coupling at optimal doping for the van Hove material when $t' = -0.19$, $U_{vH} = 1.74 t$, see Fig.3b. Away from the van Hove value of t' one obtains couplings shown in Fig.3b. For smaller values of t' corresponding to closed FS one obtains larger U but still within the range of perturbatively improved HF theory¹⁶.

The range of acceptable values of t'/t is rather limited. If one chooses $|t'|/t < 0.1$, the Mott state at very low doping does not appear²⁶. At values larger than $|t'|/t > 0.25$ the shape of the Fermi surface in the underdoped regime is qualitatively different from the one observed by ARPES. The value of $t' = -0.19t$ for Hg and Tl is chosen to tune the Lifshitz (topological) transition from the full Fermi surface to the fractured one (four arcs) occurs at experimentally observed doping $x^{opt} = 0.16$.

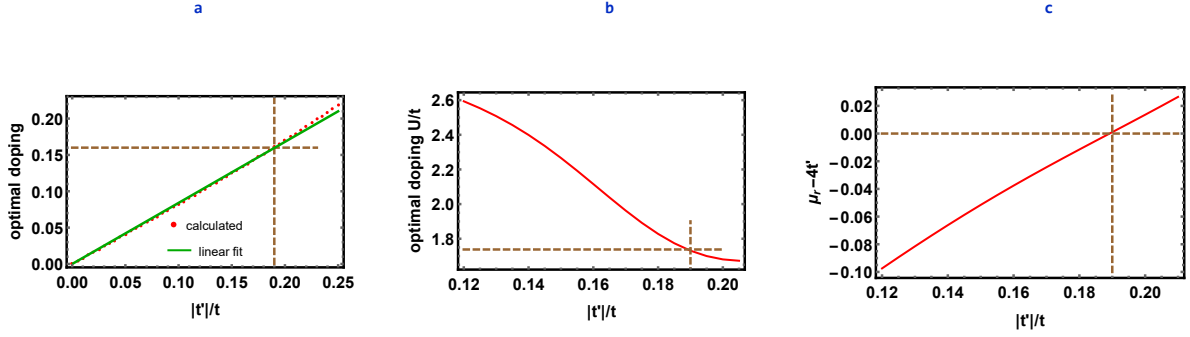


FIG. 3. a. The optimal doping as function of the ratio of hopping amplitudes t'/t . b. An effective on site Coulomb repulsion. c. Energy difference between the Fermi level and the van Hove energy.

IV. THE D-WAVE PHONON MEDIATED SUPERCONDUCTIVITY.

It is well established that phonons cause s - wave pairing in low T_c materials, however d-wave pairing is possible when forward scattering peak of Eq.(8) is present. Early work in this direction was summarized in ref.²⁷. The transition temperature T_c as function of the hole doping within the present model was studied in ref.¹³ demonstrates the maximum at p_{opt} . We start from the derivation of the phonon exchange d wave "potential" (appearing mainly near the Γ point of BZ).

A. Effective phonon generated electron - electron interactions in spin singlet channel

In order to describe superconductivity, one should "integrate out" the phonon and the spin fluctuations degrees of freedom to calculate the effective electron - electron interaction. We start with the phonons. The Matsubara action for EPI, Eq.(7), and phonons, Eq.(3), are,

$$\frac{1}{T} \sum_{m,\mathbf{q}} \left(Z e^2 n_{-m,-\mathbf{q}} g_{\mathbf{q}}^{\alpha} u_{m,\mathbf{q}}^{\alpha} + \frac{M}{2} u_{-m,-\mathbf{q}}^{\alpha} \Pi_{m,\mathbf{q}}^{\alpha\beta} u_{m,\mathbf{q}}^{\beta} \right), \quad (16)$$

where $n_{-n,-\mathbf{q}} = \sum_{\mathbf{k},m} \psi_{\mathbf{k}-\mathbf{q},m-n}^* \psi_{\mathbf{k},m}^{\sigma}$ and \mathbf{g} was defined in Eq.(8). The polarization matrix is defined via the dynamic matrix of Eq.(3): $\Pi_{n,\mathbf{q}}^{\alpha\beta} = (\omega_n^b)^2 \delta_{\alpha\beta} + M^{-1} D_{\mathbf{q}}^{\alpha\beta}$, $\alpha, \beta = x, y$. Since the action is quadratic in the phonon field \mathbf{u} , the partition function is gaussian and can be integrated out exactly, see details in ref.¹⁹. As a result one obtains the effective density - density interaction term for of electrons

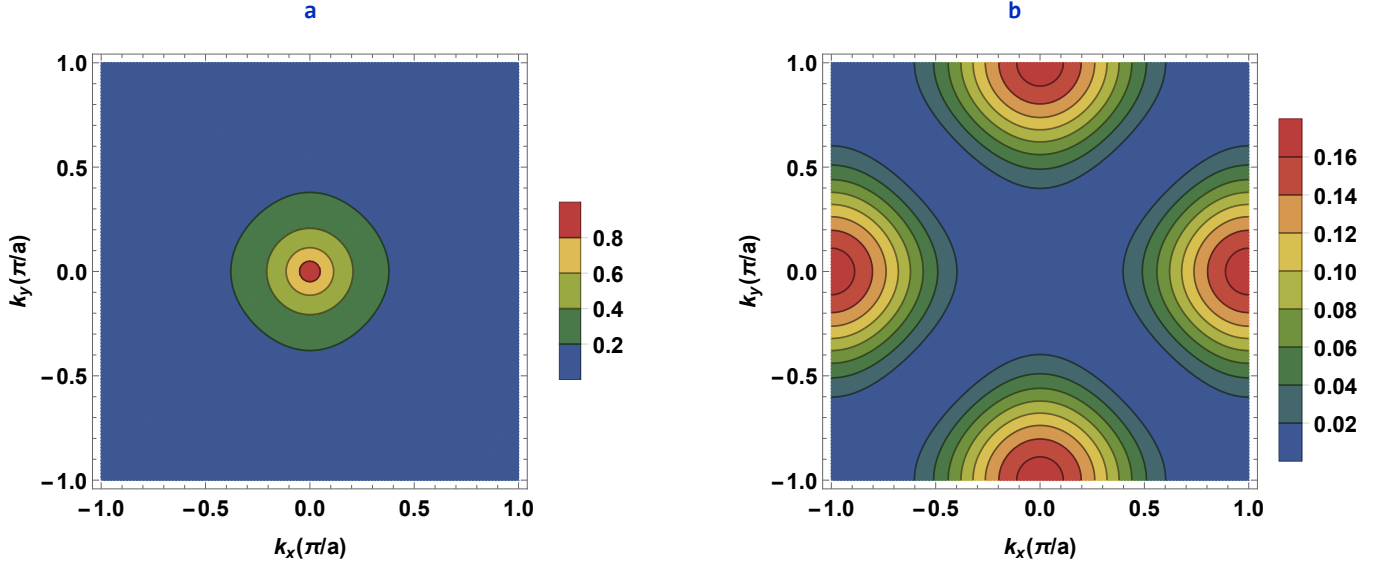


FIG. 4. a. Effective electron - electron attraction potential. Maximum at $\mathbf{q} = \mathbf{0}$ is the result of electrostatics due to the distance d_a . point. b. The effective potential for the d - wave pairing corresponding to the ALLP potential. The peak now moved to points $\mathbf{X} = (\pi/a, 0)$ and $\mathbf{Y} = (0, \pi/a)$

$$\mathcal{A}_{eff}^{ph} = \frac{1}{2T} \sum_{\mathbf{q}, n} n_{n, \mathbf{q}} V_{n, \mathbf{q}} n_{-n, -\mathbf{q}}; \quad V_{n, \mathbf{q}} = -\frac{\gamma}{\omega_n^2 + \Omega^2} e^{-2d_a |\mathbf{q}|} + U; \quad (17)$$

$$\gamma = \frac{(2\pi Z e^2)^2}{M}.$$

The central peak is clearly seen in Fig. 4a.

The standard superconducting gap equation is,

$$\Delta_{m\mathbf{k}} = -T \sum_{n\mathbf{p}} \frac{V_{m-n, \mathbf{k}-\mathbf{p}} \Delta_{n\mathbf{p}}}{\omega_n^2 + (\epsilon_{\mathbf{p}} - \mu_r)^2 + |\Delta_{n\mathbf{p}}|^2}. \quad (18)$$

Here the (Matsubara) gap function is related to the anomalous GF, $\langle \psi_{m\mathbf{k}}^\sigma \psi_{n\mathbf{p}}^\rho \rangle = \delta_{n+m} \delta_{\mathbf{k}+\mathbf{p}} \epsilon^{\sigma\rho} F_{m\mathbf{k}}$ ($\epsilon^{\sigma\rho}$ - the anti-symmetric tensor), by

$$\Delta_{m\mathbf{k}} = T \sum_{n\mathbf{p}} V_{m-n, \mathbf{k}-\mathbf{p}} F_{n\mathbf{p}}. \quad (19)$$

The gap equation was solved numerically by iteration by discretization the BZ with $N = 256$ and 64 frequencies. It converges to the d - wave solution. The absolute value of the Matsubara gap function has a maximum near the crystallographic \mathbf{X} point, $(0, \pi)$. At critical temperature the gap disappears. The values for various hopping amplitudes at optimal doping are presented in Fig.5 (as blue points). It can be fitted well by a Lorentzian (blue dashed curve):

$$T_c^{\max} = \frac{T_L}{1 + \alpha (t' - t'_L)^2}, \quad (TL)$$

with maximal value of temperature at the open to close Lifshitz point, $T_L = 92K$ achieved next to nearest hopping amplitude $t'_L/t = -0.19$. Other parameters characterizing the electron - phonon interactions, coupling U and the electron gap were given in Section II. The Coefficient α is different for $|t'| < |t'_L|$, $\alpha_< = 180$, and $|t'| > |t'_L|$, with $\alpha_> = 240$.

To understand qualitatively the results, we derive next approximate formulas for T_c in terms of the "effective" d-wave pairing strength λ_d analogous to the well known s-wave coupling λ_s . The case of the Lifshitz transition requires a special treatment near the van Hove point.

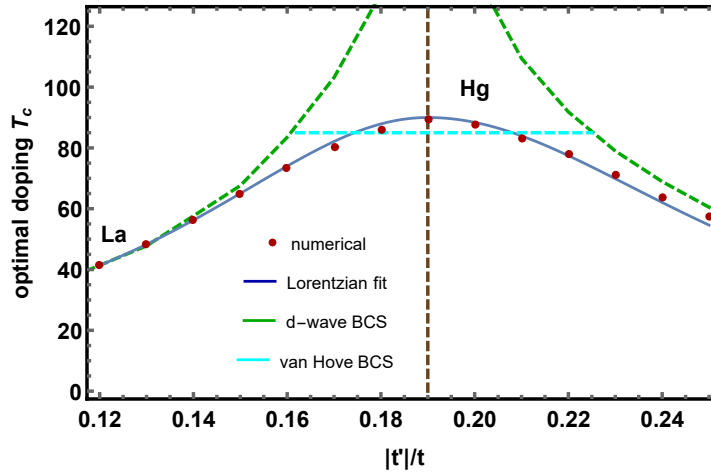


FIG. 5. Critical temperature at optimal doping as function of $t';/t$. Numerical solution is very close to the BCS formula (green dashed line) away from topological criticality. The BCS expression is "cut off" by the van Hove dominated critical value (light blue line). The numerical results are fitted by Lorentzian (blue line) given in Eq.(.).

B. The d-wave analog of the asymptotic expression for T_c

Near T_c one neglects the second term in denominator and obtains

$$\Delta_{m\mathbf{k}} = -T_c \sum_{n\mathbf{p}} V_{m-n, \mathbf{k}-\mathbf{p}} \frac{\Delta_{n\mathbf{p}}}{\omega_n^2 + (\epsilon_{\mathbf{p}} - \mu_r)^2}. \quad (20)$$

Numerical solution of the gap equation shows that the gap function decreases slowly like $1/\omega$ at large ω and is often used at intermediate coupling²⁸ and at relevant relatively small frequencies can be approximated by its $n = 0$ component:

$$\Delta_{n\mathbf{p}} = \Delta_{\mathbf{p}} = f_d(\mathbf{p}) \Delta, \quad (21)$$

The quasi-momentum dependence turns out to be quite universal:

$$f_d(\mathbf{p}) = \cos[p_x] - \cos[p_y]. \quad (22)$$

This is an analog of the BSC assumption $\Delta_{n\mathbf{p}} = \Delta$ for the s-wave. The normalization, $\sum_{\mathbf{k}} f(\mathbf{k})^2 = 1$, is convenient for the following derivation.

After multiplication of the T_c equation, Eq.(20), by $f(\mathbf{p})$ and summation over both \mathbf{p} and n , it becomes:

$$1 = - \sum_{\mathbf{p}} \frac{\rho_{\mathbf{k}-\mathbf{p}}^d}{\Omega^2} \frac{\tanh[(\epsilon_{\mathbf{p}} - \mu_r)/2T_c]}{2(\epsilon_{\mathbf{p}} - \mu_r)}. \quad (23)$$

Here

$$\rho_{\mathbf{p}}^d = f_d(\mathbf{p}) \sum_{\mathbf{k}} \rho_{\mathbf{k}-\mathbf{p}} f_d(\mathbf{k}), \quad (24)$$

is an effective form factor" of the phonon mediated interaction, see Fig.4b. For d-wave the nodal region is irrelevant, while the anti-nodal region is strongly emphasized. For the s-wave it is simpler: $\rho_{\mathbf{p}}^s = \rho_{\mathbf{p}}$.

Function $\tanh[\varepsilon/2T_c]/\varepsilon$ is peaked at $\varepsilon = 0$ with width T_c . Using steepest descent approximation (the function $\rho_{\mathbf{k}}^d$, drawn in Fig. 4b varies much slower), one arrives at:

$$1 \simeq -\frac{1}{2(2\pi)^2 \Omega^2} \int_{BZ} d^2\mathbf{p} \rho_{\mathbf{p}}^d |_{\varepsilon_{\mathbf{p}}=\mu_r} \frac{\tanh[(\varepsilon_{\mathbf{p}} - \mu_r)/2T_c]}{\varepsilon_{\mathbf{p}} - \mu_r}. \quad (25)$$

Making change of variables $\{p_x, p_y\}$ to geodesic coordinates $\{p_n, p_t\}$ (the normal and the tangential momenta), and then from p_n to $\varepsilon = \varepsilon(p_x, p_y) - \mu_r$, one obtains the BCS formula:

$$1 = \lambda^d \int_{\varepsilon=-\Omega}^{\Omega} d\varepsilon \frac{\tanh[\varepsilon/2T_c]}{2\varepsilon} \simeq \lambda^d \log \frac{2\Omega\gamma_E}{\pi T_c}. \quad (26)$$

Here the d - wave coupling constant is defined by,

$$\lambda^d = -\frac{1}{\Omega^2 (2\pi)^2} \oint_{\varepsilon} dp_t \frac{1}{v(p_t)} \rho_{p_t, \varepsilon}^d = \frac{D(\mu_r)}{2\Omega^2} \rho_{p_t, \varepsilon}^d, \quad (27)$$

where the Fermi velocity is $\mathbf{v} = \nabla\varepsilon$ and the element of length along the FS is calculated numerically as $dp_t = \sqrt{(v_y/v_x)^2 + 1} dp_y$. Finally one obtains the usual BCS - like expression for T_c :

$$T_c = \frac{2\gamma_E}{\pi} \Omega \exp\left[-\frac{1}{\lambda^d}\right]. \quad (28)$$

The values of T_c^{\max} at optimal doping are given as green lines in Fig.5. This agrees well with numerical solution of the gap equation except in the vicinity of the Lifshitz transition point at $t'_L = -0.19$ where the naive BCS T_c erroneously enters the strong coupling regime. The reason of the breakdown is that the steepest descent approximation used is invalidated near the \mathbf{X} point due to the fact that the DOS changes faster than $\tanh[\varepsilon]/\varepsilon$. In particular this leads to the logarithmically divergent density of states. Here a more sophisticated approximate calculation is required.

C. The van Hove singularity dominated critical system

In a particular case of the close to open transition at $t' = -0.19$, the FS approaches the van Hove singularity at $\mathbf{k} = (0, \pi)$ and the steepest descent approximation is invalid. However precisely in this case one can simplify the gap equation by expanding the dispersion relation around the dominant \mathbf{X} and \mathbf{Y} points. Replacing the sums by integrals in Eq.(20) and changing the variables to $\{\varepsilon = \varepsilon(p_x, p_y), p_t\}$, one obtains:

$$1 = -\frac{1}{(2\pi)^2 \Omega^2} \int_{\varepsilon=-\Omega}^{\Omega} d\varepsilon \oint_{\varepsilon} dp_t \frac{1}{v(p_t)} \rho_{\mathbf{p}}^d \frac{\tanh[\varepsilon/2T_c]}{2\varepsilon}. \quad (29)$$

This can be written via DOS, approximating $\rho_{\mathbf{p}}^d = \rho_{\mathbf{X}}^d = 0.16 \cdot \gamma$, see Fig. 4b, as

$$1 = -\frac{\rho_{\mathbf{X}}^d}{4\Omega^2} \int_{\varepsilon=-\Omega}^{\Omega} d\varepsilon \frac{\tanh[\varepsilon/2T_c]}{\varepsilon} D(\varepsilon).$$

Near the \mathbf{X} point the DOS is:

$$D(\varepsilon) = \frac{4}{(2\pi)^2 (1 + 2t'/t)^{3/2}} \ln \frac{b}{\varepsilon}; \quad (30)$$

$$b = (2\pi)^2 (1 - 2t'/t)^2 / (1 + \sqrt{2})^2.$$

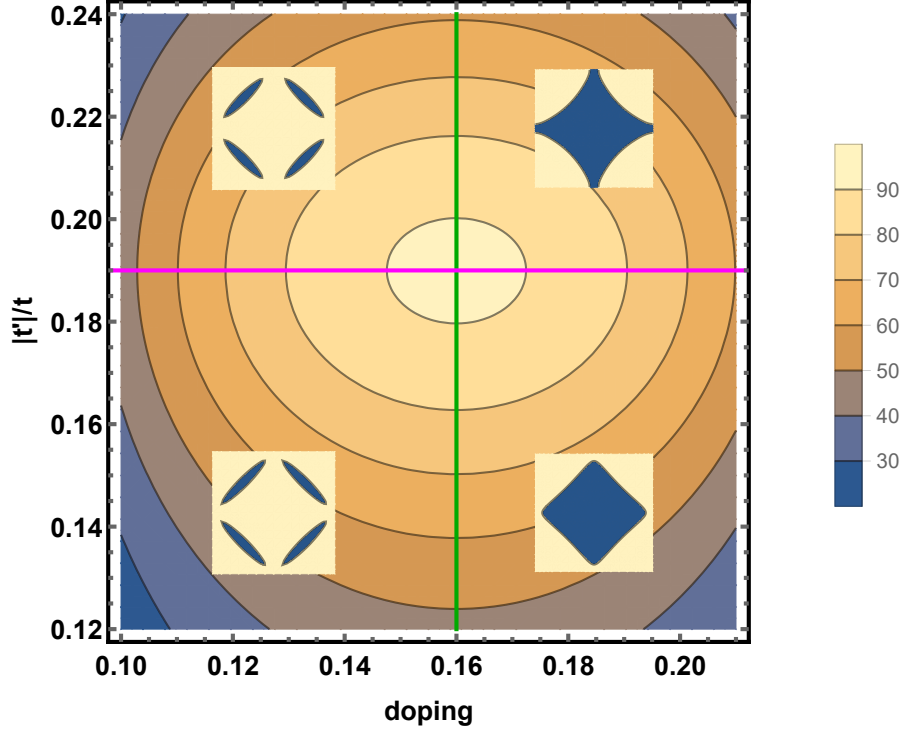


FIG. 6. The doping - hopping (t'/t) phase diagram of the single layer cuprates. Materials with very high T_c (Hg and Tl based cuprates) are described by t' slightly above the critical open - close topological transition hopping value of $t'/t = -0.19$. Lower T_c La and Bi based cuprates have much lower values around $t' = 0.12$ significantly below the transition line (magenta). Near the optimal doping $p = 0.16$ all the materials with different hopping ratios undergo the second topological transition (green) at which the open or closed Fermi surface fractures into four small pockets.

The critical temperature at the Lifshitz point ($t' = t'_L$, $\mu_r = \epsilon(\mathbf{X})$), using methods described in ref.⁹, is

$$T_c^L = t \exp \left[-\sqrt{\log^2 \frac{2t}{\Omega} + \frac{2}{\lambda_L}} \right], \quad (31)$$

where the d-wave electron - phonon coupling strength is

$$\lambda_L = \frac{|\rho_{\mathbf{X}}^d|}{(2\pi)^2 (1 + 2t'_L/t)^{3/2} \Omega^2}.$$

In the present case, $\Omega = 50 \text{ meV}$ and $t = 460 \text{ meV}$, one obtains $T_c^{\text{max}} = 82K$ (dashed light blue line in Fig. 5) compared to the numerical result $T_c^{\text{max}} = 92K$. It might be thought of as an upper cutoff on the naive d - wave BCS estimate in the topological transition region. Just slightly away from it, $|t' - t'_L|/t > 0.1$, the BCS formula works well with values of $\lambda^d = 0.4 - 0.55$.

V. DISCUSSION AND CONCLUSIONS

To conclude, large disparity of critical temperatures of one layered cuprates is explained in the framework of the apical lateral longitudinal phonon (ALLP) exchange d - wave superconductivity theory. To demonstrate the basic

principles we limited ourselves in this paper to a simple sufficiently generic model of the electron gas in the CuO planes: the fourfold symmetric $t - t'$ single band Hubbard model with on site repulsion energy U of moderate strength. It is shown that the highest T_c^{\max} materials $HgBa_2CuO_{4+\delta}$ and $Tl_2Ba_2CuO_{6+\delta}$ ($> 90K$) with a larger next to nearest neighbors hopping amplitude $t'/i \simeq 0.20$ are just above the topological transition from an open to a close Fermi surface, while $La_{2-x}Sr_xCuO_{4+\delta}$ and ($< 40K$) are well below it at $t'/t \simeq 0.12$ consistent with some first principle calculations.

As was argued in previous papers^{13,16} the values of the effective Coulomb repulsion U/t away from the Mott insulator phase should be in the intermediate coupling range, $1.5 < U/t < 3.5$, smaller than the values for the parent materials. Only in this case the pseudogap and the strange metal $d\rho/dT$ have experimentally observed order of magnitude. Here we find that U decreases monotonically with t' , see Fig. 3b. The correlation between t' and T_c^{\max} has been noticed⁴ on basis of early first principle calculations. Of course other relevant for the APPL theory parameters of the one layer cuprates, the lattice spacing a and the distance of the apical oxygen d_A from the CuO plane and the phonon frequency Ω and the apical oxygen charge Z and nearest neighbor hopping amplitude t are different. Differences in a , d_A and t are known to be very small experimentally. Less is known about the APPL electron - phonon coupling In ref.¹³ we have estimated generally the range of Ω and Z (determining the matrix element of the APPL and the CuO electron states) on the basis of a simple microscopic Born-Meyer model described in Section II. Looking at Fig.2, one notices that the Born - Meyer parameters for the apical oxygen later of the two materials are almost identical. The parameter A in Eq.(2) for La and Ba atoms are²¹ $A_{La} = 37.283eV$, $b_{La} = 3.512 A^{-1}$ and $A_{Ba} = 36.363 eV$, $b_{Ba} = 3.514A^{-1}$ respectively. As a result both Ω and Z are practically the same.

Fig. 6 summarizes the APPL theory critical temperature dependence on both doping and t' . The topological phase diagram contains two *different* Lifshitz transitions: at the critical doping p_{opt} (the green line) the FS fractures into four "pockets", while at critical next to nearest neighbor hopping $t' = t'_L$ the center of FS moves from Γ to the M point of Brillouin zone. Let us discuss some of the limitations of the present model.

One is the role of the "unconventional" spin fluctuation d - wave pairing²⁹ which at intermediate coupling might still contribute and "boost"¹³ T_c . In addition the restriction of the description of the dispersion relation to the one band Hubbard model with just two parameters t, t' for nearest neighbor and next to nearest neighbor hopping obviously makes the model less realistic to quantitatively describe real materials. If one considers adding more distant hopping terms like t'' , the condition for the topological open to close Fermi surface transitions, Eq.(11), is modified to $\mu_r = \epsilon(\{0, \pi\}) = 4t' - 4t''$. It turns out that the $t' \rightarrow t' - t''$ substitution effectively describes an effect of this more complicated dispersion relation (generally t' is negative, while t'' is positive and smaller). Of course the situation in multi layered cuprates is more involved due to inter - layer tunneling effects³⁰.

The general conclusion is the following: critical temperature of transition to superconductivity is always peaked at a topologically nontrivial (Lifshitz) restructuring of the Fermi surface. When two such transitions lines cross, see Fig. 6, the global maximum is achieved.

Acknowledgements.

We are grateful Prof. D. Li, H.C. Kao, L. L.Wang, C. Q. Jin, J.Y. Lin and Y. Yeshurun for helpful discussions. Work of B.R. was supported by NSC of R.O.C. Grants No. 101-2112-M-009-014-MY3.

- * vortexbar@yahoo.com
† shapib@biu.ac.il
- ¹ A. D. Palczewski, T. Kondo, R. Khasanov, N. N. Kolesnikov, A. V. Timonina, E. Rotenberg, T. Ohta, A. Bendouan, Y. Sassa, A. Fedorov, S. Pailhes, A.F. Santander-Syro, J. Chang, M. Shi, J. Mesot, H.M. Fretwell, A. Kaminski, /'es, A. F. Santander-Syro, J. Chang, M. Shi, J. Mesot, H. M. Fretwell, and A. Kaminski, *Phys. Rev. B* **78**, 054523 (2008).
 - ² S. W. Jang, H. Sakakibara, H. Kino, T. Kotani, K. Kuroki, and M. J. Han *Sci. Rep.* **6**, 33397 (2016).
 - ³ F. Nilsson, K. Karlsson, and F. Aryasetiawan, *Phys. Rev. B* **99**, 075135 (2019).
 - ⁴ E. Pavarini, I. Dasgupta, T. Saha-Dasgupta, O. Jepsen, and O. K. Andersen, *Phys. Rev. Lett.* **87**, 047003 (2001).
 - ⁵ D. Li, B. Rosenstein, B. Ya. Shapiro, and I. Shapiro, *Phys. Rev. B* **95**, 094513 (2017);
 - ⁶ Y. Liu, Y. J. Long, L. X. Zhao, S. M. Nie, S. J. Zhang, Y. X. Weng, M. L. Jin, W. M. Li, Q. Q. Liu, Y. W. Long, R. C. Liu, C. Z. Gu, F. Sun, W. G. Yang, H. K. Mao, X. L. Feng, Q. Li, W. T. Zheng, H. M. Weng, X. Dai, Z. Fang, G. F. Chen, & C. Q. Jin, *Sci. Rep.* **7**, 44367 (2017).
 - ⁷ A. Piriou, N. Jenkins, C. Berthod, I. Maggio-Aprile, & Ø. Fischer, *Nat. Com.* **2**, 221 (2011).
 - ⁸ J.E. Hirsch and D. J. Scalapino, *Phys. Rev. Lett.* **56**, 2732 (1986); R. Combescot and J. Labbe, *Phys. Rev. B* **38**, 262 (1988); R.S. Markiewicz, *Physica C* **217**, 281 (1993); R. J. Radtke and M. R. Norman, *Phys. Rev. B* **50**, 9554 (1994).
 - ⁹ C. C. Tsuei, D. M. Newns, C. C. Chi, and P. C. Pattnaik, *Phys. Rev. Lett.* **65** 2724 (1990)
 - ¹⁰ S. Raghu, S. A. Kivelson, and D. J. Scalapino, *Phys. Rev. B* **81**, 224505 (2010).
 - ¹¹ B.-X. Zheng, C.-M. Chung, P. Corboz, G. Ehlers, M.-P. Qin, R. M. Noack, H. Shi, S. R. White, S. Zhang, and G. K.-L. Chan, *Science* **358**, 1155 (2017); K. Ido, T. Ohgoe, and M. Imada, *Phys. Rev. B* **97**, 045138 (2018); H.-C. Jiang, and T. P. Devereaux, *Science* **365**, 1424 (2019); M. Qin, C.-M. Chung, H. Shi, E. Vitali, C. Hubig, U. Schollwöck, S. R. White, and S. Zhang, *Phys. Rev. X* **10**, 031016 (2020).
 - ¹² G. Rohringer, H. Hafermann, A. Toschi, A. A. Katanin, A. E. Antipov, M. I. Katsnelson, A. I. Lichtenstein, A. N. Rubtsov and K. Held, *Rev. Mod. Phys.* **90** 025003 (2018); P. Pudleiner, A. Kauch, K. Held and G. Li, *Phys. Rev. B* **100**, 075108 (2019); T. Schafer, N. Wentzell, F. Simkovic, Y.-Y. He, C. Hille, M. Klett, C. J. Eckhardt, B. Arzhang, V. Harkov, F.-M. Le Regent, A. Kirsch, Y. Wangl, A. J. Kimm, E. Kozik, E. A. Stepanov, A. Kauch, S. Andergassen, P. Hansmann, D. Rohe, Y. M. Vilck, J. P. F. LeBlanc, S. Zhang, A.-M. S. Tremblay, M. Ferrero, O. Parcollet, and A. Georges, "Tracking the Footprints of Spin Fluctuations: A Multi-Method, Multi-Messenger Study of the Two-Dimensional Hubbard Model", arXiv:2006.10769v2 (2021).
 - ¹³ B. Rosenstein and B.Ya. Shapiro. *J. Phys. Com.* **5**, 055013 (2001)
 - ¹⁴ N. Bulut and D. J. Scalapino, *Phys. Rev. B* **45**, 2371 (1992); T. P. Devereaux, T. Cuk, Z.-X. Shen, and N. Nagaosa, *Phys. Rev. Lett.* **93**, 117004 (2004); C. Honerkamp, H.C. Fu and D.-H. Lee, *Phys. Rev. B* **75**, 014503 (2007).
 - ¹⁵ S. Johnston, F. Vernay, B. Moritz, Z.-X. Shen, N. Nagaosa, J. Zaanen, and T. P. Devereaux, *Phys. Rev. B* **82**, 064513 (2010); Z. B. Huang, Lin H. Q. and E. Arrigoni, *Phys. Rev. B* **83** 064521 (2011).
 - ¹⁶ H. C. Kao, D. Li, and B. Rosenstein, "Unified approach to the pseudogap and the strange metal phases of cuprates" (2021).
 - ¹⁷ C. Falter, M. Klenner, and Q. Chen, *Phys. Rev. B* **48**, 16690 (1993); C. Falter and F. Schnetgoke, *Phys. Rev. B* **65**, 054510 (2002); C. Falter, *Phys. Stat. Sol.* **242**, 78 (2005).
 - ¹⁸ B. Rosenstein, D. Li, T. X. Ma, and H.C. Kao, *Phys. Rev. B* **100**, 125140 (2019).
 - ¹⁹ B. Rosenstein and B. Ya. Shapiro *Phys. Rev. B* **100**, 054514 (2019).
 - ²⁰ Q. Song, T. L. Yu, X. Lou, B. P. Xie, H. C. Xu, C. H. P. Wen, Q. Yao, S. Y. Zhang, X. T. Zhu, J. D. Guo, R. Peng, D. L. Feng et al, *Nature Com.* **10**, 758 (2019).
 - ²¹ A. A. Abrahamson, *Phys. Rev.* **178**, 76 (1969).
 - ²² L. P. Gor'kov, *Phys. Rev. B* **93**, 060507(R) (2016)
 - ²³ Evarestov R. A. ,*Quantum Chemistry of Solids*, Second Edition, London Springer Series in Solid-State Sciences **153** (2012).
 - ²⁴ T.A. Maier, A. Macridin, M. Jarrell, and D.J. Scalapino, *Phys. Rev. B* **76** 144516 (2007).
 - ²⁵ J. W. Furness, Y. Zhang, C. Lane, I. Gianina Buda, B. Barbiellini, R. S. Markiewicz, A. Bansil, J. Sun, *Commun. Phys.* **1**, 11 (2018).
 - ²⁶ P. A. Igoshev, M. A.Timirgazin, V. F. Gilmudtinov, A. K. Arzhnikov and V. Yu. Irkhin *J. Phys. Cond. Mat.* **27** 446002 (2015).
 - ²⁷ M. L. Kulić, *Phys. Rep.* **38**, 1 (2000).
 - ²⁸ A. T. Rømer, T. A. Maier, A. Kreisel, I. Eremin, P. J. Hirschfeld, and B. M. Andersen, *Phys. Rev. Research* **2**, 013108 (2020).
 - ²⁹ A. Eberlein, and W. Metzner, *Phys. Rev. B* **89**, 035126 (2014); R. Misuno, M. Ochi, and K. Kuroki, *J. Phys. Soc. Jap.* **86**, 114706 (2017); A. Taheridehkordi, S. H. Curnoe and J. P. F. LeBlanc, *Phys. Rev. B* **102**, 045115 (2020); F. Šimkovic, Y. Deng, and E. Kozik, *Phys. Rev. B* **104**, L020507 (2021).
 - ³⁰ S. Benhabib, A. Sacuto, M. Civelli, I. Paul, M. Cazayous, Y. Gallais, M.-A. Méasson, R. D. Zhong, J. Schneeloch, G. D. Gu, D. Colson, and A. Forget, *Phys. Rev. Lett.*, **114**, 147001 (2015).